TEST RESULTS OF HYTEM A MORPHING TRAILING EDGE DEMONSTRATOR

J. TIKALSKY, M. RADESTOCK*

*Institute of Lightweight Systems, German Aerospace Center (DLR)
Lilienthalplatz 7 Braunschweig, Germany
e-mail: jan.tikalsky@dlr.de, web page: http://DLR.de/

Abstract.

The aviation industry's biggest challenge is transitioning to climate neutrality by reducing reliance on fossil fuels. As a result, aerodynamic efficiency has become the primary focus of future aircraft designs.
Morphing trailing edges can improve lift-to-drag ratios, particularly in off-design conditions. However, current solutions often require slitting the wing's pressure side, resulting in gaps that negatively impact aerodynamic performance. To address this issue, a novel approach uses a compliant mechanism in the trailing edge, driven by a conventional kinematic system.
A demonstrator was manufactured and tested, showing good correlation between analytical and finite element calculations. However, initial operation revealed softening due to the Mullins effect, causing deviations from predicted static loads. Fatigue testing based on flight data showed slow crack propagation, meeting aviation requirements.
The pre-design methods used have proven suitable, and the system's crack behavior meets aviation standards. As next step a new demonstrator will be developed to investigate spanwise differentiation of the hyperelastic trailing edge morphing (HyTEM) system. The HyTEM system will be implemented on the unmanned aerial system (UAS) PROTEUS platform and undergo flight tests to evaluate improvements in lift-to-drag ratios achieved through morphing trailing edges.
Key words: Morphing, Wing, Trailing Edge, HyTEM

1 INTRODUCTION

Trailing Edge Morphing (TEM) has been extensively researched over the years, but none of these technologies have been adopted for use in commercial aircraft. However, research conducted in the late 1980s and early 1990s by [1–3] demonstrated that camber morphing can achieve benefits of up to 20% on fighter-type aircraft.

Transonic passenger aircraft were also investigated in the 80s and 90s (see [4, 5]), with studies suggesting a potential increase in lift-to-drag ratio (L/D) by 2-3% when using variable camber on Fowler flaps. Further research by Vale et al. [6] showed that spanwise camber morphing can offer an additional 2% improvement in L/D.

Despite this promising research, only a handful of TEM designs have been tested in flight to date [7]. These designs are subject to stringent requirements for load-bearing and flexibility, which necessitates the use of heavy actuators and sophisticated kinematics. This complexity results in increased manufacturing costs, maintenance expenses, and safety assessments.

This paper presents a new design principle for implementing a camber-variable morphing system, known as Hyperelastic Trailing Edge Morphing (HyTEM). The concept will be introduced first, followed by a description of Demonstrator A. The third section will focus on static testing of the Demonstrator and compare theoretical predictions with test results. Followed by a description of a Cyclic fatigue test and its results.

1.1.Hyperelastic Trailing Edge Bonding Concept

The biggest challenge for morphing designs is the wing skin, which undergoes changes in length due to deformation. This results in large internal loads, making it essential to develop a solution that can mitigate these loads.

To address this issue, Figure 1 shows a stiff and continuous skin (15,16) which are bonded elastically (17) at the skin connection between pressure and suction side. This allows a seamless transition of the profile surface into the deformable area without material changes throughout the profile body.

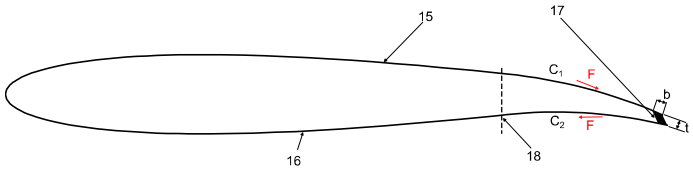

Figure 1: HyTEM Wingsection Concept [8]

The connection between the trailing edge is achieved through a compliant joint made from hyper-elastic adhesive Sika-Pro3 (surface 17 in Figure 1).

This design enables the integration of variable shape trailing edges into conventional composite airfoil designs while maintaining step-free transitions and minimizing gaps. Moreover, it is feasible to have the variable shape area start at different chord length on the upper and lower sides via stiffness differences, allowing to tilt the hinge line (18).

Figure 1 also shows the connection line (18) between the fixed and flexible region of the airfoil.

Due to its high elasticity at the trailing edge, the cross-section of the Flexible area exhibits torsional softness, enabling the curvature of the profile to generate differentiated deflections along the span. Figure 2 shows a sketch where the cross-sections at root and tip deflect downwards, while the middle cross-section deflects upwards.

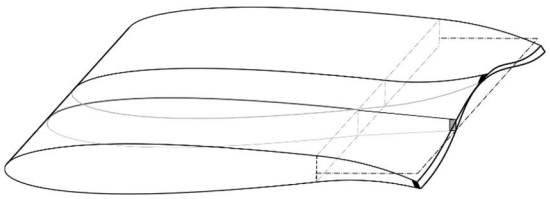

Figure 2: HyTEM spanwise differential excitation [9]

The spanwise differentiation can then be utilized to optimize lift distribution depending on the flight operation point, offering an aerodynamic potential to reduce total drag. One objective of DLR's ongoing project MorphAIR [10] is to develop and test such a spanwise differential morphing concept using an unmanned aerial system (UAS). This approach aims to minimize drag by manipulating the shape of the wing.

Due to the nature of this system, strain energy increases with deformation (displacement) of the trailing edge. The HyTEM is designed as a multifunctional lifting surface to replace ailerons and flaps. This requires fast movements around zero deflection to mimic aileron properties and overcome large as well as slow movements while being deployed as a flap.

To minimize the weight of the actuator, a non-linear transmission is required. A direct transition in the neutral position and a small transmission ratio in the deployed position are necessary to achieve this goal. Figure 3 shows the kinematic with a rotational actuation as scheme.

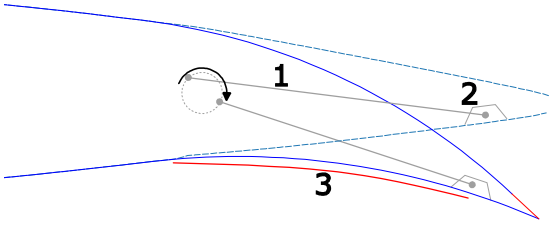

Figure 3: HyTEM Kinematic concept [9]

The kinematic concept for HyTEM involves an excentre attached to a rotary actuator, which is hinged to a pushrod (1). The pushrod itself is hinged to a load introduction bracket close to the trailing edge. This design aims to unload area 3 from compressing loads, thereby avoiding buckling and reducing skin bending Stiffness, which in turn reduces strain energy required for system operation.

For more details, refer to [11] , which proposed a demonstrator description.

1.2.Demonstrator Setup

The concept is intended to fly on the UAS Proteus to investigate performance increases. A demonstrator according to the Proteus design has been developed and fabricated. The most challenging area of the UAS is the close-to-root section, where flaps will be extended maximally. Additionally, aileron functionality is incorporated in this region. Figure 4 shows the Proteus fuselage with the right wing. The cut section is the selected airfoil geometry for the demonstrator in full-scale.

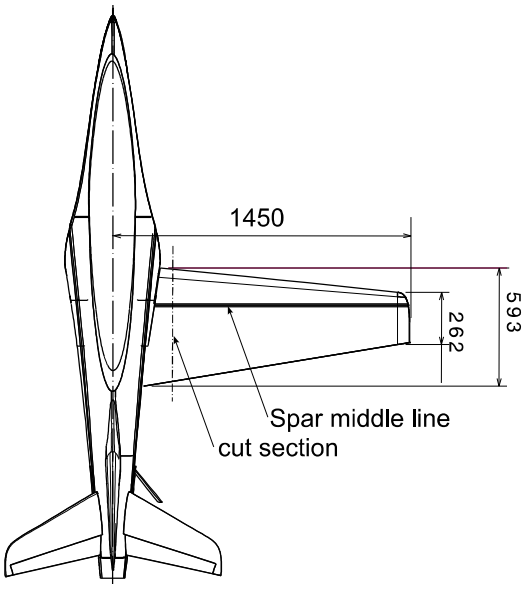

Figure 4: Demonstrator A wing cut section [9]

For simplification purposes, the profile at the trailing edge is replaced by flat plates and do not represent the airfoil curvature. These plates are attached to the main spar. Figure 5 shows the CAD model of the demonstrator cross-section with simplified plates, spar, actuator and pushrod for actuation. Also, the airfoil geometry is plotted over the CAD model in order to give an impression of the deviation for the trailing edge simplification.

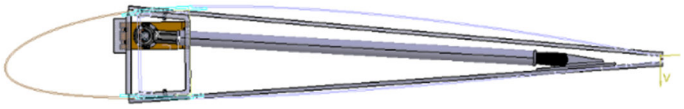

Figure 5: CAD model of the Demonstrator A and cross section of the airfoil [9]

The top view in Figure 6 gives the impression of the 100mm span segment of the demonstrator. Furthermore, this figure show the actuator positioning in orange, because it is not parallel to the spar middle line, which poses a problem for the actuator alignment in the final wing. In the demonstrator A design, the actuator is tilted to accommodate this issue.

Figure 6: Top view of demonstrator A with actuator in orange [9]

The main dimensions of demonstrator A can be found in Figure 7, and additional properties such as skin layup are presented in [11].

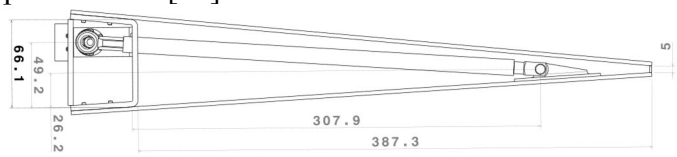

Figure 7: Side view with dimensions [9]

A loadcell has been installed in the pushrod to enable direct force measurements. The demonstrator is prepared for testing, with a bracket installation shown in Figure 8. A small distance between the pushrod and upper skin can be recognized.

Figure 8 is a detailed photo of demonstrator A rear end with the bracket. The tests with demonstrator A will be performed also with masses on the Pressure side of the demonstrator. This allows easier investigations of a flap deflection behavior and the reaction to loads. A small distance (no contact) between Pushrod and upper skin can be recognized.

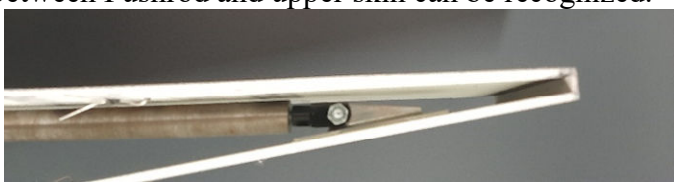

Figure 8: Detailed photo of Demonstrator A with bracket on upper side

Two configurations have been tested. Configuration 1 has a actuator rotational angle of Φ_0 90 degree and Configuration 2 has a Φ_0 of 138 degree, where the angle definition is shown in Figure 9.

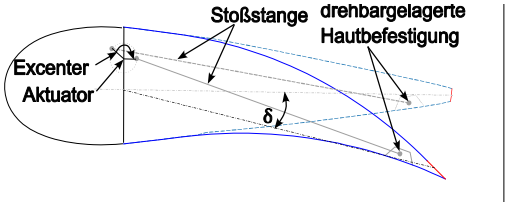

Figure 9: kinematics definition

1.3.Static tests

Within this section focuses on the validation of the FEM as well as analytical model of the system. In a first step the demonstrator in configuration 1 has been 3d scanned with an ATOS

system in undeformed and deformed condition (Figure 10). This system scans the surface with stereographic cameras and an optical fringe pattern.

Figure 10: ATOS Measurement setup

These scanned surfaces were compared to the original CAD design and the results from the deformed FEM calculations shown in Figure 11.

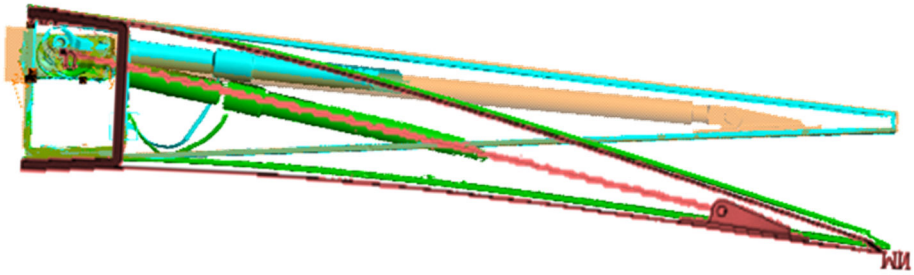

Figure 11: ATOS measurement in deflected position (green) compared to CAD model (orange) and ATOS measurement in undeflected position (turquoise) compared to FE Model (Red)

Good correlation was observed between the experimental data and the analytical predictions. The maximum deviation of deformation is by 1,3% between the measured deformation and the predicted deformation by FE model.

Another focus lies on predicting the pushrod load at the excentre position without external loads. An experiment was performed using configuration 2, where a slow sine movement of the excentre between -45° and +50° was carried out. Pushrod forces and excentre positions where recorded.

Figure 12 shows the overlay of deformed and undeformed Demonstrator.

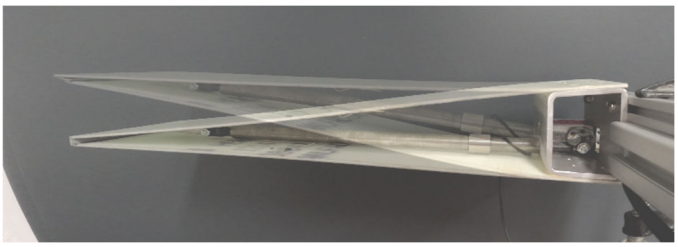

Figure 12: Demonstrator Static measurement without external loads Config. [-45° - 50°]

Figure 13 shows the measurements, the FEM and the analytically predicted pushrod forces in dependence of the excentre position. A hysteresis of the measured pushrod loads can be found in the measurements. This hysteresis can be explained by viscoelastic material behavior in the hyperelastic adhesion.

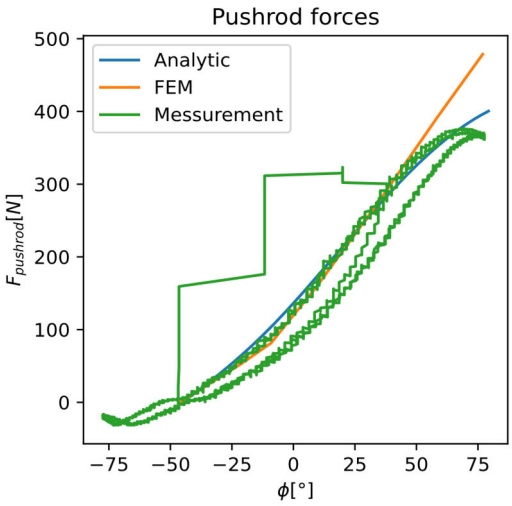

Figure 13: Pushrod measurement over excentre position without external loads

Good correlation between FE predictions and measurement (deviation <4%) was found within this range -45° to +50°, but the FE solution overestimated the pushrod loads for higher angles. In contrast, the analytical solution showed a high correlation between -46° and +60°.

Figure 13 shows the predicted pushrod force over flap deflection, revealing that for small deformations, FEM predicts smaller loads than measured, whereas higher deformations show the opposite trend. The analytical prediction is quasi-linear due to its geometrical and material simplifications.

In case that the analytical solution approximates the measurement data more precise then the FE results, the comparison indicates that the material properties of the adhesive used in this test case are not accurately captured. The analytical material model is conducted from coupon tests to extract linearized material properties. Further characterization on nonlinear Neo Hookean Material properties is needed to improve the FEM accuracy. However, the comparison between measurement, numerical solution and analytical approach show a usable application for first estimation of the Hytem concept in the design process.

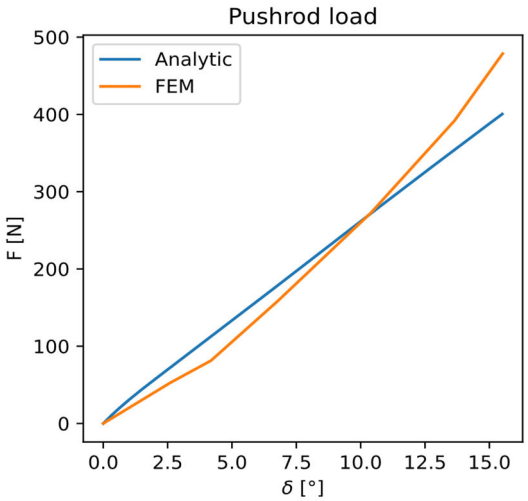

Figure 14: Pushrod forces over flap deflection

Figure 15 shows the actuator and predicted moment over the rotational angle, highlighting that the measurement data may be too coarse for use in flight measurements. This can be attributed to the friction of installed gears, which limits the precision of the actuator internal measurement results. An application scenario for tracking the push rod forces is a health monitoring system for the adhesive. Due to the coarse data such a monitoring system seems to be to inaccurate.

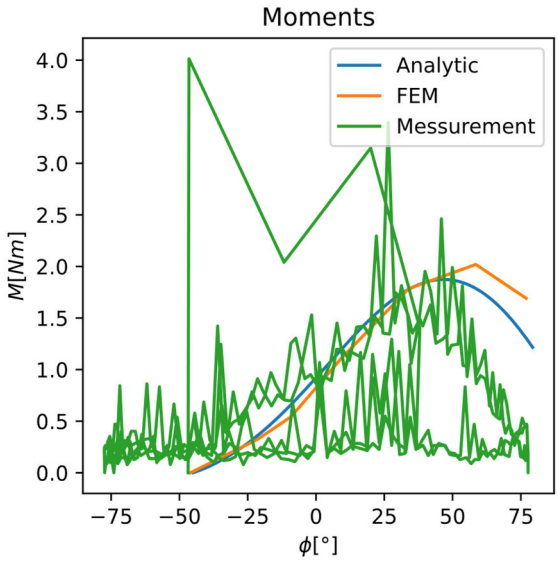

Figure 15: Actuator Moment over angle

2 FATIGUE STRENGTH TEST

The cyclic tests follow a similar structure to static tests. Photos were taken at the end of each cycle to assess crack growth. Before starting the fatigue strength test, 12 cycles were conducted to calibrate the measuring system and CAN-BUS, as well as perform earlier mentioned static tests. The focus is on damage growth, ensuring suitability for flight testing.

To investigate operational stability, a load spectrum from Proteus flights was determined instead of a single-stage test procedure. Figure 16 shows a test cycle including portions mimicking take-off and landing. The morphing trailing edge will be used as multifunctional system so that the cycles are prepared to represent flaperon behavior. For limiting test times ailerons deflections are multiplied by 5 to generate a conservative estimate of maximum load on the wing's root.

The load spectrums amplitude increases at the start (0-35 seconds) and end due to landing (318-360 seconds) flaps and reduced speed. Additionally, control inputs for course correction can be observed in cruise flight (35-318 seconds). This procedure provides a conservative estimate, as no flight test data are available yet. For the fatigue test the load spectrum is repeated until break of the adhesive.

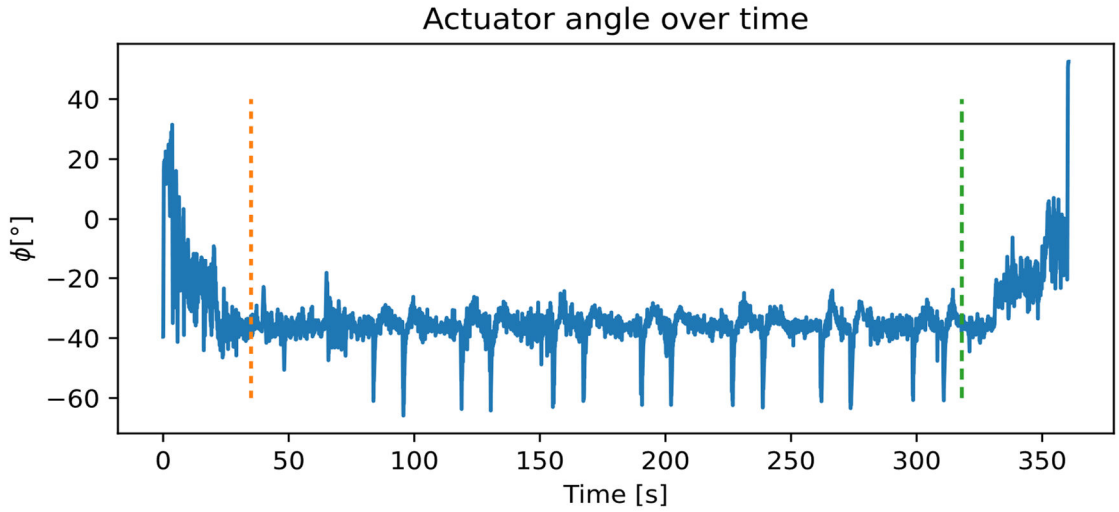

Figure 16: Assumed load Collective

Figure 17 shows the measured pushrod force at sequence time 360s per sequence. The curve declines throughout the investigation. Sample photos (A-F) are presented in Figure 20-25 to observe crack initiation and growth.

At the beginning of the test (Point A), no macro cracks can be detected. The first crack appears at Point B (16.6% of lifetime), consistently growing until Point C (71.3% of lifetime). After Point C, new cracks emerge and grow to Point D (~80% of lifetime). The forces decline steadily up to this point. However, after 80%, the bonding degradation accelerates.

Even if an early crack occurs, the system can still be qualified for flight testing. Cracks in the adhesive can be easily detected and repaired if needed. Between the first crack initiation(B)

and accelerated bonding degradation (D) is about 60% of lifetime to identify and repair the crack. Even after (D) 20% of cycles has been performed before fatal fraction.

The load collectives can then be derived using the measurement data from later flights, resulting in a more accurate determination of actual service life using a higher number of tests and geometries.

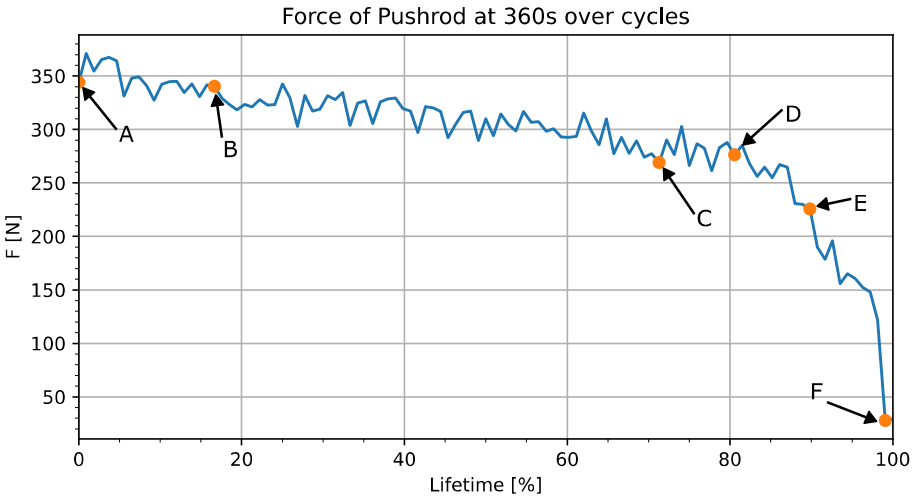

Figure 17: Pushrod force over cycles at 360s sequence time

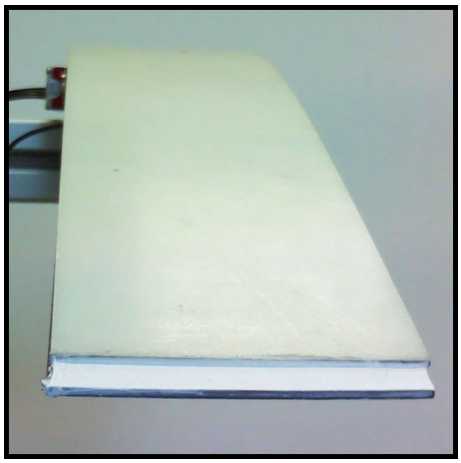

Figure 18: Point A 0%

Figure 19: Point B 16,6%

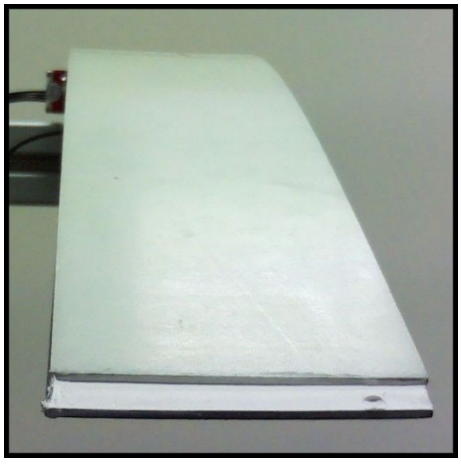

Figure 20: Point C 71,3%

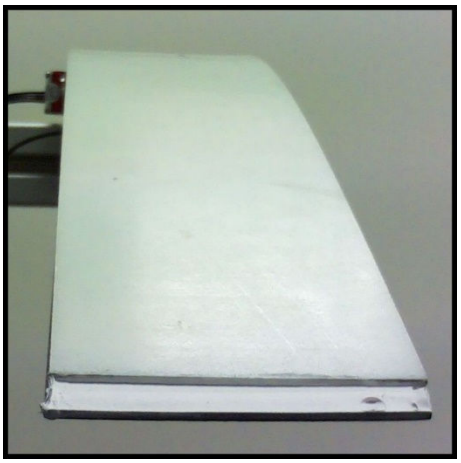

Figure 21: Point D 80,6%

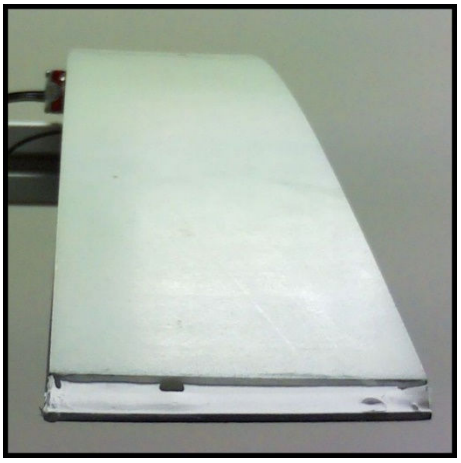

Figure 22: Point E 89,8%

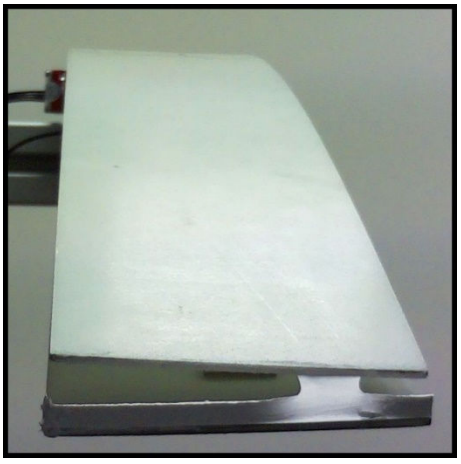

Figure 23: Point F 99%

3 SUMMARY AND OUTLOOK

This work demonstrated the suitability of HYTEM for flight testing through the construction, static and cyclic testing of a HYTEM-based demonstrator A. The results showed that both analytical and Finite Element (FE) modeling provided excellent predictions for static loads on the pushrod and overall deformation. Therefore, these methodologies can be used to assess the design of an hyperelastic trailing edge morphing concept.

Furthermore, slow crack growth was observed in the cyclic tests, which is a crucial indicator of failure-relevant cracks. This finding ensures that such cracks can be detected and repaired during pre-flight inspections, enhancing safety.

Looking ahead, cyclic Test sequence has to be adopted using flight test data. The cyclic tests have to be repeated and analyzed to conduct a more precise lifetime. Using the actual sudden increased degradation could open the possibility to establish a self-monitoring method.

The following demonstrator B with 5 actuator stations and spanwise differentiated deflections will be investigated concerning load interactions. Following this, HYTEM will be integrated into a morphing wing for the MorphAIR project and undergo flight testing, marking an important milestone in its development.

References

[1] AFWAL-TR-88-3082, ed., AFTI/F-111 Mission Adaptive Wing Briefing to industry. Final Report, 1988.
[2] John W. Smith, wilton P. Lock, Gordon A. Payne, “Variable-Camber Systemsintegration and Operational Performance of the AFTI/F-111 Mission Adaptive Wing: NASA Technical Memorandum 4370,” NASA Technical Memorandum 4370, 1992.
[3] Sheryll Goecke Powers, Lannie D. Webb, Edward L. Friend, William a. Lokos, “Flight Tests Results From a Supercritical Mission Adaptive Wing With Smoth Variable camber: NASA Technical Memorandum 4415,” NASa Technical Memorandum, No. 4415, 1992.
[4] Greff, “Stand der Aerodynamik-Arbeiten zum FFE-Vorhaben "Funktion des Intelligenten Flügels" (Status of aerodynamic works for FFE "Function Of Intelligent Wings"),” 21 Jan. 1991.
[5] “SIP-Projekt: Flügel Variabler Wölbung (Wing Of Variable Chamber),” TK 62/099/92, 10.1992.
[6] do Vale, J. L., Afonso, F., Lau, F., and Suleman, A., “Span Morphing Concept: An Overview,” Morphing Wing Technologies, Elsevier, 2018, pp. 125–144.
[7] Barbarino, S., Bilgen, O., Ajaj, R. M., Friswell, M. I., and Inman, D. J., “A Review of Morphing Aircraft,” Journal of Intelligent Material Systems and Structures; Vol. 22, No. 9, 2011, pp. 823–877. doi: 10.1177/1045389X11414084.
[8] Jan Tikalsky, elastische Hinterkantenverklebung(Elastic Trailing edge Bonding), DE 10 2023 117 337 B3, 30.06.2023.
[9] Jan Tikalsky, “HYTEM DEMONSTARTOR: DESIGN AND ANALYSIS OF A MORPHING TRAILING EDGE DEMONSTRATOR USING HYPERELASTIC ADHESIVE,” ASME SMASIS 2024 [online], Vol. 2024; SMASIS2024-140049, https://doi.org/10.1115/SMASIS2024-140049, [retrieved 30 January 2025].
[10] M.Radestock, DLR UAS TEST PLATFORM FOR MORPHING WINGS, Austin (TX), USA, September 2023.
[11] Jan Tikalsky, “Morphing Compliant Trailingedge Skin Concept,” 09/2023.